HAL
open science

Thermal Stability of Oleate-Stabilized Gd2O2S Nanoplates in Inert and Oxidizing Atmospheres

Clément Larquet, D. Hourlier, Anh-Minh Nguyen, Almudena Torres-Pardo, Andrea Gauzzi, Clément Sanchez, Sophie Carenco

▶ **To cite this version:**

Clément Larquet, D. Hourlier, Anh-Minh Nguyen, Almudena Torres-Pardo, Andrea Gauzzi, et al.. Thermal Stability of Oleate-Stabilized Gd2O2S Nanoplates in Inert and Oxidizing Atmospheres. ChemNanoMat, 2019, 5 (4), pp.539-546. 10.1002/cnma.201800578 . hal-02017819

HAL Id: hal-02017819

https://hal.sorbonne-universite.fr/hal-02017819v1

Submitted on 13 Feb 2019

HAL is a multi-disciplinary open access archive for the deposit and dissemination of scientific research documents, whether they are published or not. The documents may come from teaching and research institutions in France or abroad, or from public or private research centers.

L'archive ouverte pluridisciplinaire **HAL**, est destinée au dépôt et à la diffusion de documents scientifiques de niveau recherche, publiés ou non, émanant des établissements d'enseignement et de recherche français ou étrangers, des laboratoires publics ou privés.

Thermal stability of Oleate-Stabilized Gd_2O_2S Nanoplates in Inert and Oxidizing Atmospheres

*Clément Larquet,[1,2] Djamila Hourlier,[3] Anh-Minh Nguyen,[1] Almudena Torres-Pardo,[4] Andrea Gauzzi,[2] Clément Sanchez,[1] Sophie Carenco[1,]**

[1] Sorbonne Université, CNRS UMR 7574, Collège de France, Laboratoire de Chimie de la Matière Condensée de Paris (LCMCP), 4 place Jussieu, 75005 Paris, France

[2] Institut de Minéralogie de Physique des Matériaux et de Cosmochimie (IMPMC), Sorbonne Université, CNRS UMR 7590, IRD UMR 206, MNHN, 4 place Jussieu 75252 Paris Cedex 05, France

[3] Institut d'Electronique, de Microélectronique et de Nanotechnologie (IEMN), UMR 8520, Avenue Henri Poincaré, BP 60069, F-59652 Villeneuve d'Ascq Cedex, France

[4] Departamento de Química Inorgánica, Facultad de químicas, Universidad Complutense, 28040-Madrid, Spain

* Corresponding author e-mail: sophie.carenco@sorbonne-universite.fr

Abstract: Capping ligands play an important role in the chemistry of nanoparticles synthesized in organic surfactants. This is relevant to a number of device applications where heating may cause major modifications of crystalline nanoparticles including amorphization, surface rearrangements or sintering. Ultrathin monodisperse $Ln_2O_2S_x$ oxysulfide nanoparticles (Ln = lanthanide) obtained in a mixture of oleylamine, oleic acid and 1-octadecene show promising luminescence and light absorption properties. In view of applications, one open question concerns the thermal behavior and the role of the ligands on the thermal reactivity of the nanoparticles.

In this report, we show that the thermal stability of $Gd_2O_2S_x$ nanocrystals is limited because of their non-stoichiometric composition and strongly depends on the annealing atmosphere. The sintering temperature of the nanoparticles is lower in air than in inert atmosphere because of a rapid degradation of the ligands. Annealing the nanoparticles in air enables to remove the ligands without altering the nanocrystals structure. The decomposition of the $Gd_2O_2S_x$ nanocrystals in inert atmosphere exhibits a complex multi-step behavior that can be precisely modeled. This work gives a comprehensive description of the stability conditions of lanthanide oxysulfide nanoparticles. It establishes the range of conditions for their practical use and opens the way to major improvements of the surface activity of Ln_2O_2S nanoparticles and related nanocrystals.

Keywords: Gadolinium oxysulfide nanoparticles, organic ligands, structural stability, thermogravimetric analysis, mass spectrometry.

1. Introduction

Owing to their tunable optical emission and absorption properties, lanthanide oxysulfides Ln_2O_2S (Ln = lanthanide and yttrium) have found applications in various devices such as phosphors for cathode ray tubes,[1–4] scintillators,[5–7] and lasers (emission[8–10] and absorption[11,12]). Following the first studies carried out in the 60's on the synthesis, morphology and doping of bulk samples, these compounds have been recently obtained also in the form of nanoparticles by means of various synthesis routes. This progress has renewed the hype for lanthanide oxysulfides, because these nanoparticles are promising for bimodal imaging (magnetic and optical), a key technology in nanomedicine.[13]

Ln_2O_2S nanoparticles are synthesized either in an aqueous or organic medium, which requires two different sulfidation methods. In water, sulfidation is performed in a subsequent step by heating the precursors at high temperature (T> 600 °C) using either sulfur vapor,[14–16] CS_2 formed *in situ* (S_8 in carbon)[17,18] or H_2S.[19] In organic medium, sulfidation is achieved at milder temperatures and in a single step. For instance, in a mixture of oleylamine, oleic acid and 1-octadecene, $Ln(acac)_3$ reacts with elemental sulfur at 310 °C in inert atmosphere. Oleylamine helps dissolving the elemental sulfur and forming reactive sulfide species.[20] With the help of an alkaline source, Ln_2O_2S nanoplates surrounded by organic ligands are obtained.[21–24]

One open question concerns the thermal stability of nanoscaled Ln_2O_2S, a factor that may limit the practical use of these nanomaterials. For instance, the absorption of light (X-rays in scintillators, visible light for laser absorption) is often accompanied by strong local heating. Owing to the high-temperature sulfidation process, the nanoparticles obtained in aqueous medium are typically larger than 50 nm and their crystal structure is similar to that of the bulk phase.[25–27] This accounts for a high thermal stability up to 1200 °C observed for most lanthanides (cerium excluded).[28]

On the other hand, the small Ln_2O_2S nanocrystals (below 30 nm) obtained in organic media differ markedly from bulk crystals. Typical feature are the non-stoichiometry,[29] the presence of alkyl-chains at the surface[21] and the capability of self-assembling into wires[30]. For example, gadolinium oxysulfide easily form small non-stoichiometric $Gd_2O_2S_x$ nanoplates (8 nm x 1.5 nm) with x = 0.4 - 0.6, which self-assemble in solution into nanowires.[21,22]

In this report, we studied the thermal stability of gadolinium oxysulfide nanoparticles covered with organic ligands in inert and oxidizing atmospheres. In inert atmosphere, we discovered a multi-step behavior with temperature that leads to the phase segregation of bulk oxysulfide Gd_2O_2S and Gd_2O_3. This is explained by the non-stoichiometry ($x \neq 1$) of the $Gd_2O_2S_x$ nanocrystals. Thanks to Fourier transform infrared spectroscopy (FTIR) and thermogravimetric analysis coupled with mass spectrometry (TGA-MS), we were able to determine the nature of the ligands, their amount on the surfaces of the nanocrystals and their coordination modes on the surface gadolinium atoms.

Under oxidizing atmosphere, a few steps of transformation lead to the formation of both bulk gadolinium oxide and gadolinium oxysulfate. Moreover, we could isolate ligand-free nanoparticles by controlling the thermal decomposition of the ligands in oxidizing atmosphere. This process removes the highly hydrophobic character of the nanocrystals, and makes them suitable for practical use, eg. in water or biological media.

2. Results and discussion

Gd_2O_2S nanoparticles synthesis and structure

Gd_2O_2S nanoparticles were synthesized following an optimized protocol described in the experimental section and previously reported by our group.[22] Briefly, $Gd(acac)_3 \cdot xH_2O$ (0.5 mmol) was mixed with elemental sulfur (0.5 equiv. S *vs.* Gd), Na(oleate) (1 equiv. *vs.* Gd) in a mixture of oleylamine, oleic acid and 1-octadecene. The reaction was conducted at 310 °C for 30 minutes and yielded the nanoparticles presented in Figure S1.

The Gd_2O_2S nanoparticles crystallize in the *P-3m1* hexagonal space group. The anisotropic growth leads to the formation of hexagonal-shaped platelets of 7.8 ± 1.3 nm width and 1.5 ± 0.2 nm thickness, i.e. two to three unit cells thick. The S:Gd ratio is ca 0.25, hence much lower than that in the bulk phase, as reported by Ding *et al*.[21] and by our group[22]. This result is explained by the presence of organic ligands at the surface that stabilize $[Gd_2O_2]^{2+}$ terminal layers on the {001} facets of the lamellar compounds. The sample composition is thus better described by the formula $Gd_2O_2S_{0.5}$. For the sake of clarity and consistency with previous published works (by us and others), we will keep below the notation Gd_2O_2S that best represent the crystal structure.

Thermal stability of Gd_2O_2S nanoplates in inert atmosphere

The thermal stability of the Gd_2O_2S nanoplates was analyzed by thermogravimetric analysis (TGA) coupled with mass spectrometry in inert atmosphere (He). The results of the TGA in inert atmosphere are presented in Figure 1.

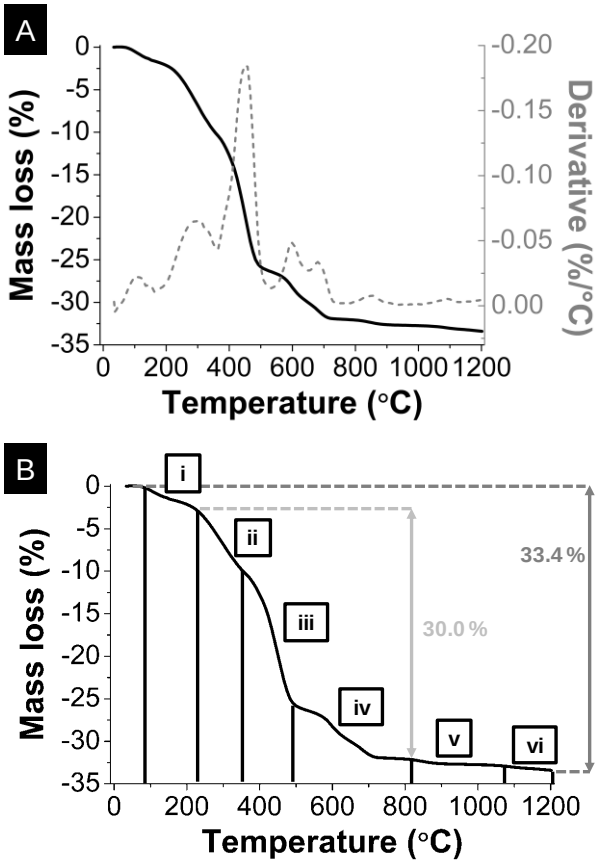

Figure 1: (A) Thermogravimetric analysis of Gd_2O_2S nanoplates performed in inert atmosphere at 2 °C/min and its temperature derivative. The curve is divided into six steps each corresponding to a partial mass loss (B).

Thermal decomposition of Gd_2O_2S nanoparticles is a complex process that can be divided into at least six steps, as shown in Figure 1B. The total mass loss between 25 °C and 1200 °C is 33.4 %. One third of the sample was lost in the form of volatile species during the heating. The combination of mass spectrometry with the TG equipment allowed us to precisely identify the various gas species emitted during each step (Figure 2).

Remarkably, the chemical processes are well separated. For the sake of clarity, only major volatile products detected are shown in Figure 2.

(i) From 40 to 210 °C: $\mathbf{H_2O}$ (*m*/*z* 18, 17, 16) + CO_2 (*m*/*z* 44, 28, 16, 12)

(ii) From 210 to 360 °C: $\mathbf{CO_2}$ (*m*/*z* 44, 28, 16, 12)

(iii) From 360 to 490 °C: hydrocarbon species $\mathbf{C_xH_y}$ (from alkyl chains of ligands) + CO_2 + CO (*m*/*z* 28, 16, 12) + H_2O

(iv) From 560 to 710 °C: 2 substeps: $\mathbf{CO_2}$ + CO first, then only **CO**

(v) From 780 to 900 °C: **CO**

(vi) From 1020 to 1120 °C: $\mathbf{H_2S}$ mainly (*m*/*z* 34, 33), and traces of H_2O

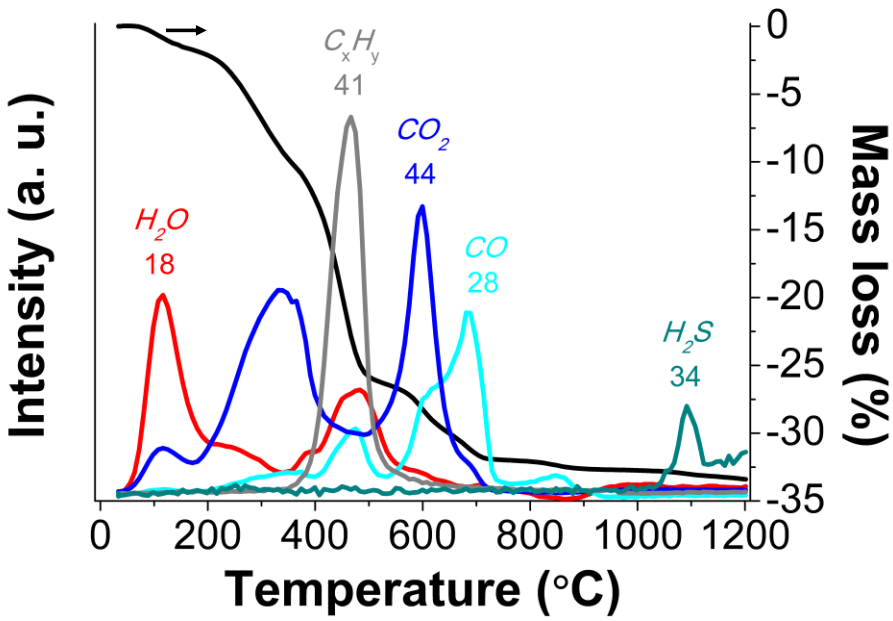

Figure 2: Thermal evolution of the major fragments detected in the gas phase by mass spectrometry: H_2O (*m*/*z* 18), CO (*m*/*z* 28), H_2S (*m*/*z* 34), C_3H_5 (*m*/*z* 41) and CO_2 (*m*/*z* 44).

The loss of water and CO_2 around 100 °C is attributed to physisorbed molecules. The emission of these species is expected, considering that the condensation of acetylacetonate ligands on oleylamine during the synthesis generates H_2O *in situ* and considering that the samples were isolated and washed in ambient air (Figure 1B step (i)).[31]

In step (ii), the decarboxylation of oleate molecules starts and CO_2 is formed. The liberation of CO_2 alone must involve oleate groups in which the terminal functionality –(COO–) is rather labile and susceptible to decarboxylation. It seems reasonable to suppose that a certain number of COO groups are farther away from the Gd sites and thus decarboxylated at this step (free oleic acid and weakly bonded oleate), while others oleate molecules remain strongly

bonded to the surface of the nanoparticles. We put forward the hypothesis that the alkyl chains of the oleate molecules decarboxylated in step (ii) remain bonded to the other oleate groups that are still coordinated to the surface gadolinium (no C_xH_y signature at this step). The long alkyl chains may be bonded either by weak interactions between the hydrophobic chains or covalently by reaction *via* the C–C double bonds.

In step (iii), a major decomposition of organic-based ligands occurs, resulting in the detection of numerous fractions related to long alkyl chains. Evidence for this is the release of a set of fragments at *m/z* 41, 55, 43, 69, 81 shown in Figure 3, resulting from the scission of the oleate ligands followed by hydrogen radical recombination. The main ion at *m/z* 30 characteristic of oleylamine is absent of the mass spectrum, which indicates that there is no significant amount of oleylamine *vs.* oleates on the surface of the nanoparticles.[32]

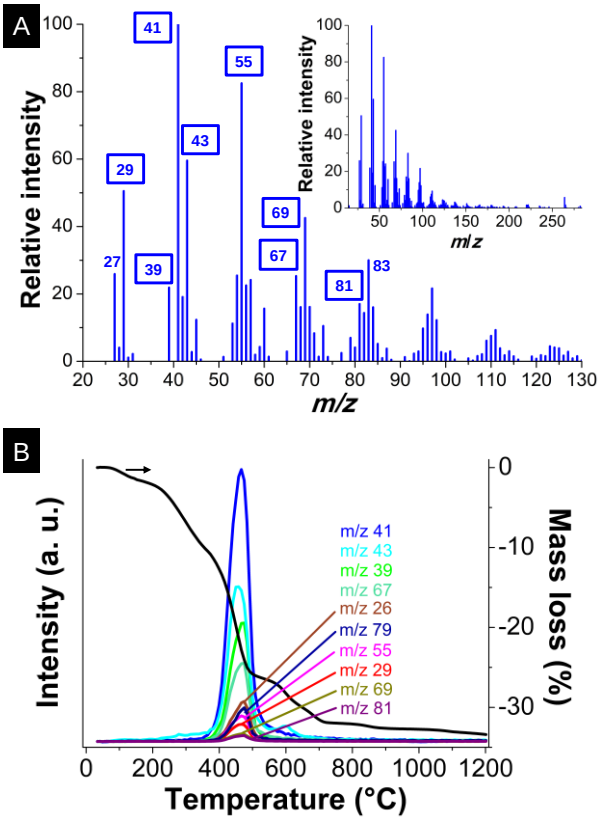

Figure 3: (A) Oleic acid mass spectrum with *m/z* between 20 and 130, from the NIST database.[33] The inset displays the total spectrum. (B) Thermogramm of Gd_2O_2S nanoplates

and detected fractions of hydrocarbon species of ligands. Framed numbers in (A) correspond to fractions detected in (B).

It is well known that the organic ligands decomposition provides not only volatile molecules, but also a carbonized solid residue called free carbon. It results from cracking of the organic chains and recombination of radicals. This degradation step causes the most important mass loss in step (iii), along with the loss of CO_2, CO and H_2O. The decarboxylation goes on and the formed CO_2 can react with the free carbon to yield CO according to the Boudouard reaction: $CO_2 + C = 2\ CO$. CO and H_2O can also form by decarbonylation of carboxylate moieties during the ligand decomposition.

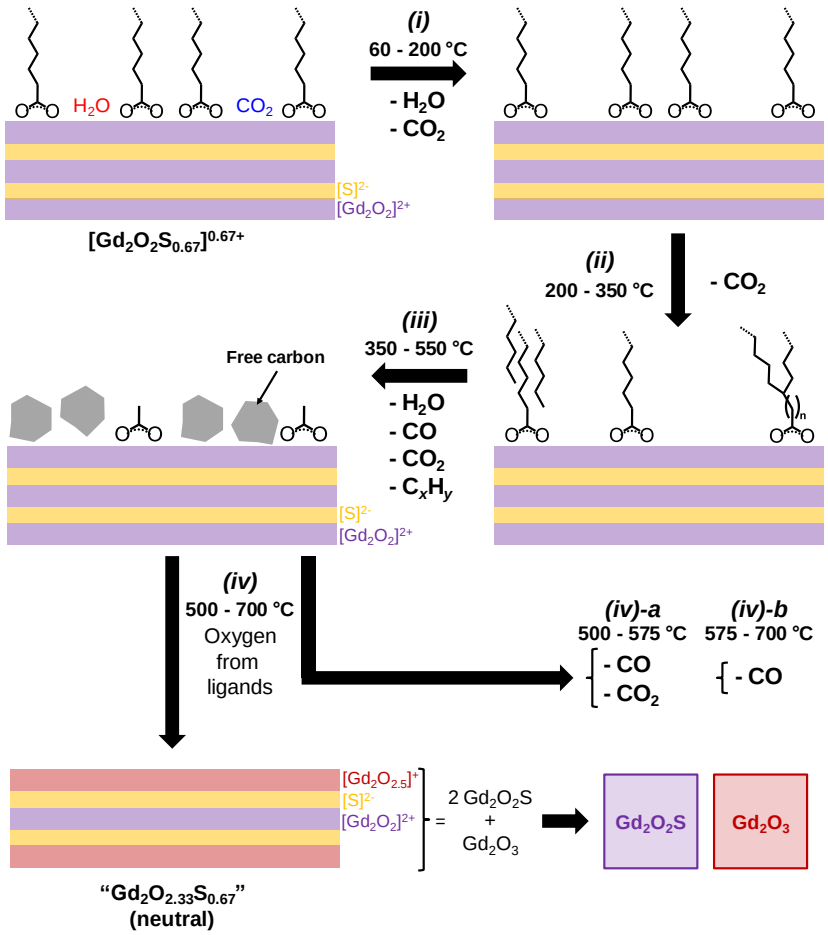

Figure 4: Proposed mechanism of the thermal decomposition during the annealing of Gd_2O_2S nanoplates (steps (i) to (iv)).

There are two crucial points here. First, during steps (ii) and (iii), ligands undergo important modifications: the charge balance can still be ensured by the remaining carboxylates groups. In the meantime, the surface becomes more accessible and thus sintering becomes easier (Figure 4).

Second, as the crystals grow and sinter, the lack of sulfur in the powder makes the formation of larger crystals of stoichiometric Gd_2O_2S impossible. The formation of large crystals of non-stoichiometric $Gd_2O_2S_{\sim 0.5}$ is prohibited as charge balance would not be respected in this case (there are no more ligands to compensate the charge). We could also imagine that the free carbon at the surface of the crystals could limit the sintering process. However, we observe at high temperatures (> 900 °C) the coexistence of growing crystals of Gd_2O_2S with allotropes of Gd_2O_3 on the XRD patterns of the annealed powders (Figure S2).

Step (iv) can be divided in two sub-steps regarding the evolution of the fragments corresponding to CO_2 and CO (Figure 2). Carbon dioxide comes from the end of the decarboxylation process. Carbon monoxide is likely the product of the reaction between the free carbon (formed by the decomposition of the ligands carbon chains in step (iii)) and CO_2 according to the Boudouard reaction. The equilibrium favors the formation of CO at high temperatures, which could explain that CO becomes the major product in (iv)-*b* (Figure 2B).

At the same time, oxygen from the ligands necessarily feeds the surface of the nanoparticles to maintain charge balance. The carboxylate groups coordinated on the surface form C–O–Gd bonds. Upon heating, a number of the C–O bonds break, leaving excess oxygen on the surface (Figure 4). $[Gd_2O_2]^{2+}$ terminal layers become $[Gd_2O_{2.5}]^{+}$ (red layers in Figure 4) while the ligands decompose. The average formula for the resulting nanoplate turns from $[Gd_2O_2S_{0.67}]^{0.67+}$ to neutral $Gd_2O_{2.33}S_{0.67}$. In parallel, the phase separation and growth lead to large crystals of Gd_2O_2S and Gd_2O_3.

Step (v) , from 780 to 900 °C, represents a limited mass loss induced by evolved CO, possibly formed at the previous step but adsorbed on Lewis acid sites. Step (vi) corresponds to a loss of a small quantity of H_2S coming from a limited degradation of the oxysulfide phase. The TG analysis associated to the structural investigations by XRD (Figure S2) indicates that the heat treatment up to 1200 °C did not significantly affect the different compositions (Gd_2O_2S, Gd_2O_3-c and Gd_2O_3-m) between the end of step (v) and that of step (vi).

Ligand nature, amount and coordination

The previous section showed that oleates are the most significant ligands (if not the only ones) around the nanoparticles. Their amount was estimated to be around 30 wt% of the powder of Gd_2O_2S nanoplates. Infrared spectroscopy was then employed to determine the chemical bonds present in the nanopowders. A representative IR spectrum of Gd_2O_2S nanoplates is displayed in Figure 5. The main absorption bands are due to the oleate ligands: 2959 cm^{-1} (CH_3 asymmetric elongation); 2923 cm^{-1} (CH_2 asymmetric elongation); 2853 cm^{-1} (CH_2 symmetric elongation); 1497 cm^{-1} (COO asymmetric stretching); 1385 cm^{-1} (COO symmetric stretching).

The frequency difference between the asymmetric and symmetric stretching bands of the COO group is indicative of the bonding type of the carboxylate ligand. In particular, Deacon and Phillips[34] indexed more than eighty acetate or trifluoroacetate compounds whose crystalline structures and infrared spectra were available, according to the acetate coordination type: unidentate ligand, chelating ligand, bridging bidentate ligand and monoatomic bridging ligand (Figure 5B).

For the nanoparticles studied here (Figure 5A), the difference between the two stretching modes of COO group is $\Delta\nu = 112$ cm^{-1} ($\nu_{asym} = 1497$ cm^{-1} and $\nu_{sym} = 1385$ cm^{-1}). In comparison, the values measured on sodium oleate are $\Delta\nu = 100$, 118 and 139 cm^{-1} (separation of the symmetric band in three contributions, see Figure S3). The low value of $\Delta\nu$

(< 150 cm^{-1}), close to the value of the corresponding sodium carboxylate, is typical of chelating or bridging carboxylate ligands, and rules out the monodentate ligand configuration (Figure 5B, coordination mode I). Moreover, in comparison with the numerous structures presented by Deacon and Philips, this value is one of the lowest, and suggests that chelation is favored in our case (Figure 5B, coordination mode II).

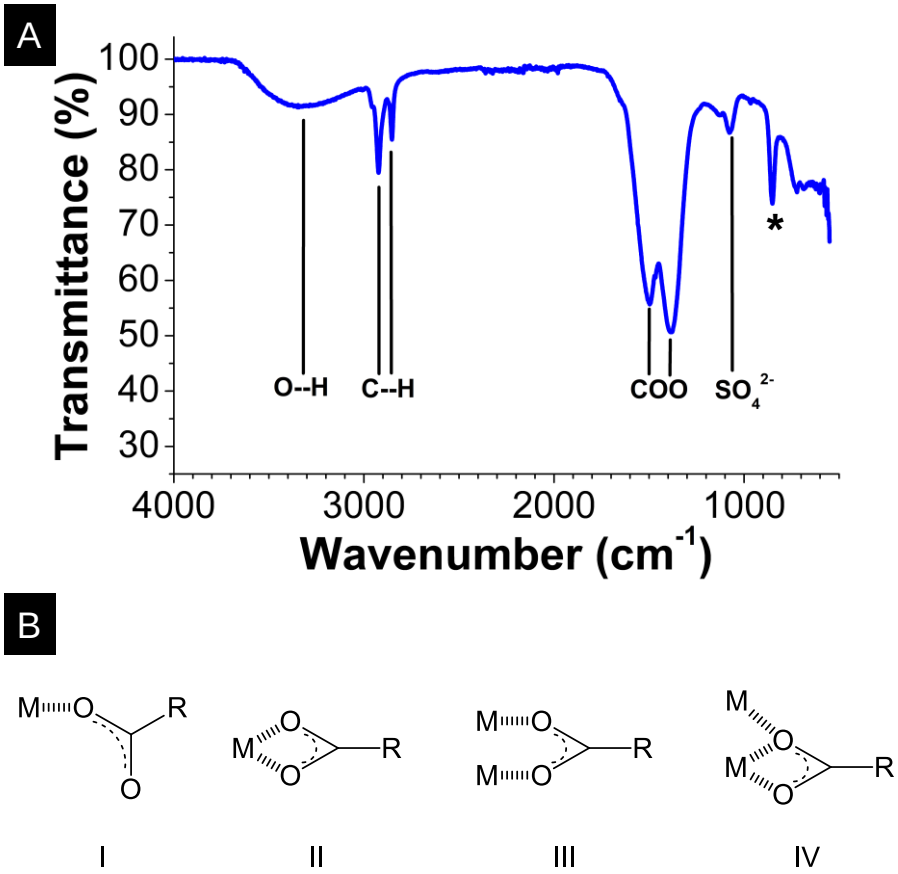

Figure 5: (A) FTIR spectrum of Gd_2O_2S nanoplates collected in ATR mode. The peak at 850 cm^{-1} is under investigation. (B) Four coordination modes between a carboxylate ligand and a metal as references by Deacon and Phillips: monodentate (I), chelating (II), bridging bidentate (III) and monoatomic bridging (IV).[34] Geometric derivatives mixing different bonding types also exist and are not presented.

On the basis of thermogravimetric analysis, the calculated amount of ligands is around 30 wt% of the Gd_2O_2S nanoparticles powder. It is thus possible to estimate the ratio between

the quantity of oxygen coming from the oleate ligands and the exposed gadolinium of our nanoplates, considering the nanoplate geometry (Figure S1).

We based this estimation on the average mass of powder obtained per synthesis: 100 mg fractioned between 3 mg of lightly adsorbed products (including water, step (i) in Figure 2), 30 mg of oleate ligands and 67 mg of $Gd_2O_2S_x$ nanocrystals. Because only 40 % of the gadolinium of the nanoplates is exposed to the surface (both {100} and {001} facets), we calculated that each gadolinium atom monopolized 1.43 oxygen atoms from the oleate ligands (Figure S4). For such a value, a mix between chelation (two oxygen atoms per metallic cation) and bridging (one O per M) can be envisaged. This result is in agreement with the structures of lanthanide carboxylates (from samarium to lutetium[35] and yttrium[36]) for which the IR signals evidenced a ratio of 2 chelating ligands for 1 bridging ligand (total: 1.6 O/Ln).

However, with this ligand quantity, the charge compensation is not reached. If we assume the $Gd_2O_2S_{0.5}$ formula for the nanoparticles (+ 1 total charge), they should be surrounded by 1 equiv. of oleate ligands (- 1 charge per molecule) to obtain the charge balance. Here, approximately 0.72 oleate ligand per Gd_2O_2S surrounds the nanocrystals, which is not enough. Nevertheless, one should remember that the oleate ligands are mainly bonded to gadolinium atoms by chelation. It means that there is not much remaining space for an additional ligand to bond a metal. Actually, the number of oleate ions represents a spatial occupation of 4.5 ligands/nm^2, which is already a high value for such ligands (values in the literature are closer to 0.2 nm^2 for each –COO$^-$ group).[37,38] Accordingly, Anderson *et al.* reminded that the steric hindrance between the alkyl chains of the oleate will limit the coverage to the density of crystalline alkyl chains (4.9 chains/nm^2).[39,40]

In this first part, we described the thermal behavior of the nanoparticles annealed under inert atmosphere. This allowed us to identify the nature and to estimate the number of organic ligands surrounding the nanoparticles. However, technological use of such nanoparticles will

likely include heating devices under ambient atmosphere. To model these conditions, we performed a second analysis in flowing gas containing a mixture of helium and 20 % O_2 in volume.

Thermal behavior under oxidizing atmosphere and ligand removal

The thermal behavior of Gd_2O_2S nanoplates was also investigated under oxidizing atmospheres with an air-like mixture (O_2/He with 20/80 *v/v*) and at intermediate reaction temperatures, in order to identify the nature of the solid formed at the most relevant steps.

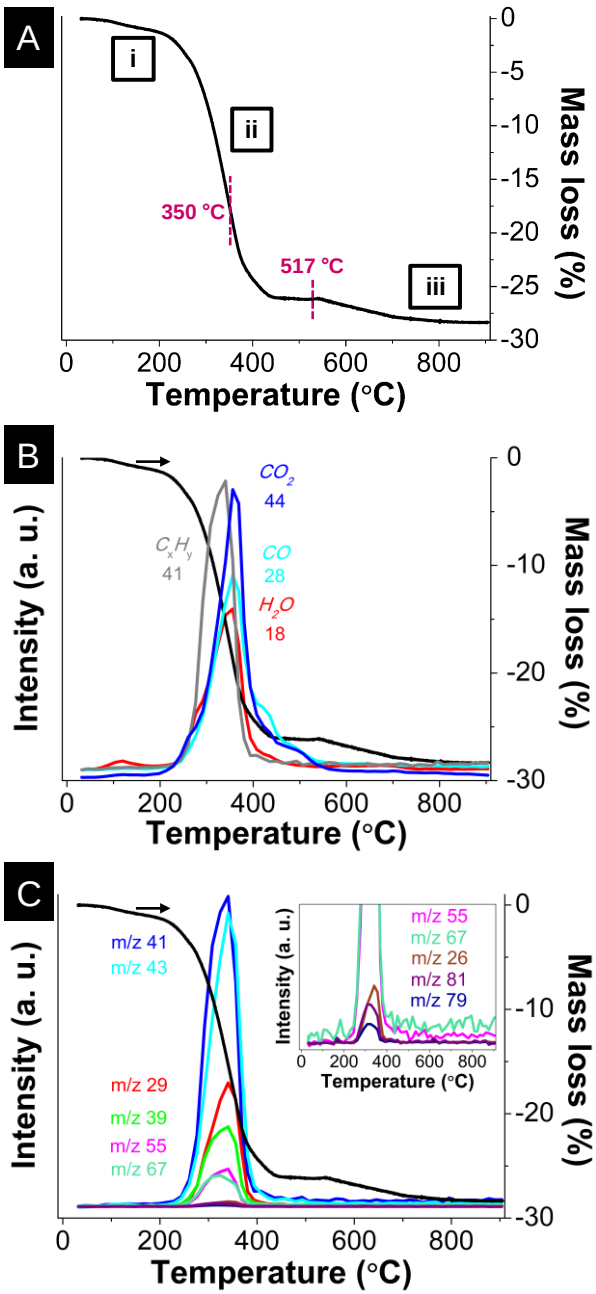

Figure 6: Thermal behavior of Gd_2O_2S nanoplates under oxidizing atmosphere. Evolution of the mass (A) and fragments from mass spectrometry: (B) H_2O (*m/z* 18), CO (*m/z* 28), C_3H_5 (*m/z* 41), CO_2 (*m/z* 44) and (C) various C_xH_y species.

Under O_2/He (20/80 *v/v*), the final mass loss is lower than in inert atmosphere (Figure 6). This is due to the formation of gadolinium oxysulfate $Gd_2O_2SO_4$, detected by XRD (Figure 7). These compounds are known to form from oxysulfides in oxidizing medium (reversible

reaction possible in H_2) and were shown to be promising for thermally activated oxygen storage.[41]

It is worth noting that the thermal decomposition in oxygen observed in the TGA curve (Figure 6) occurs in three steps. The first mass loss between 40 °C and 200 °C is quite similar to that obtained in inert atmosphere, and corresponds to the loss of physisorbed species H_2O and CO_2. The major mass loss of 25 % occurs in the second step between 250 °C and 400 °C. The last step above 500 °C implies a moderate 4 % loss of the sample mass.

In order to identify the intermediate compounds, we performed two additional experiments for which we stopped the heating ramp at selected temperatures: 350 °C (within step (ii) in Figure 6A) and 517 °C (after the end of step (ii)). The temperature was kept constant for twenty minutes before cooling down and collecting the powder. When heated around 350 °C for 20 minutes, although the ligands have undergone considerable changes, the resulting product still corresponds to Gd_2O_2S nanocrystals (Figure 7B), as attested by the broadness of the XRD peaks which is similar to these of the starting material. TEM confirmed this by showing the presence of small polycrystalline aggregates as well as still isolated nanoparticles in the sample (see Figure S6). Infrared spectroscopy after this 20 min plateau confirms that the alkyl chains are not detected anymore (Figure S3).

In comparison, the same thermal treatment at 517 °C led to nanoscaled powders majorly consisting of gadolinium oxide. For higher temperatures, XRD indicates that the oxysulfide phase completely disappears as a result of the oxidizing treatment. It may form an amorphous intermediate first, while part of the product crystallizes into cubic gadolinium oxide (Gd_2O_3-cubic). Then the amorphous part crystallizes into gadolinium oxysulfate (Figure 7A).

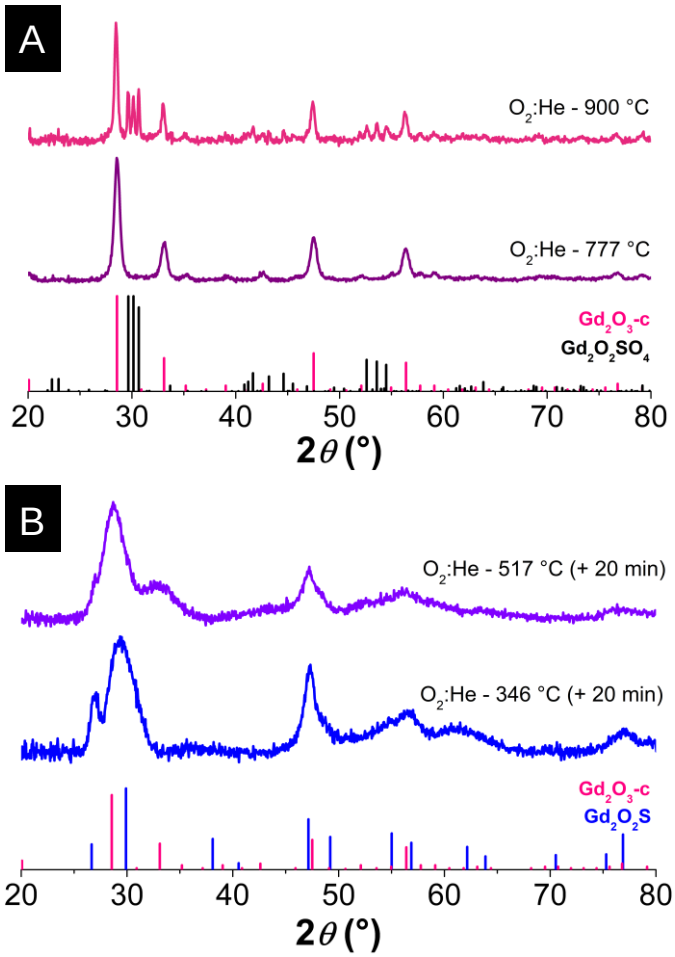

Figure 7: Powder XRD patterns of annealed Gd_2O_2S nanoplates under O_2:He (20/80 *v/v*), (A) at 900 °C (pink) and 777 °C (purple), (B) 517 °C (violet) and 346 °C (blue). In (A) the heating was stopped once the target temperature was reached. In (B), the target temperature was maintained for 20 min before cooling down. XRD pattern references are JCPDS files 26-1422 (Gd_2O_2S, blue), 12-0797 (Gd_2O_3-cubic, pink) and 77-9842 ($Gd_2O_2SO_4$, black).

In this section, we demonstrated that the inorganic crystal of Gd_2O_2S is stable up to around 350 °C under oxidizing atmosphere. The nanoscale is also preserved at this temperature. It is thus possible to remove the surface ligand at this temperature without degrading the inorganic core of the nanoparticles.

Conclusion

Many analytical techniques have been employed to monitor the thermal stability of Gd_2O_2S nanoplates stabilized by organic ligands. Our results demonstrate that the thermal stability critically depends upon the surrounding atmosphere. In inert atmosphere, the degradation of the nanoplates follows a multi-step process associated with a variety of mechanisms (dehydration, decarboxylation, ligand degradation, decarbonation/decarboxylation and sintering) that lead to distinct mass losses. In oxidizing atmosphere, the various reactions occur simultaneously at lower temperatures. The sulfur-defective structure of the nanocrystals triggers off the formation of gadolinium oxide crystals as well as oxysulfide or oxysulfate species depending on the atmosphere.

The above study enabled us to better characterize the surface species present on the nanocrystals. Our analysis rules out the possibility of a significant amount of amide ligands derived from oleylamine chains and shows that only oleate groups cover the nanoparticle surface. The oleate groups are coordinated at gadolinium surface atoms in both chelation and bridging modes.

In the present study, we demonstrated that the hydrophobic oleate chains are readily removed by a mild treatment at 350 °C in oxygen, which does not alter the nanoplate properties. This smooth process may be useful in view of the practical applications of these nanomaterials as thin films for lightening devices or post-functionalization with hydrophilic ligands for biomedical applications.

Experimental section

Synthesis of Gd_2O_2S nanoparticles

Gadolinium oxysulfide nanoparticles were prepared under inert atmosphere in a mixture of organic solvents following a previous report.[22] Oleylamine (OM; technical grade, 70 %), oleic acid (OA; technical grade, 90 %), sulfur (S_8; ≥ 99.5 %) and sodium oleate (Na(oleate); ≥ 99 %) were purchased from Sigma-Aldrich. 1-Octadecene (ODE; technical grade, 90 %) was purchased from Acros Organics. Gadolinium acetylacetonate hydrate ($Gd(acac)_3 \cdot xH_2O$; 99.9 %) was purchased from Strem Chemicals. All products were used as received without further purification.

In a typical synthesis of Gd_2O_2S, $Gd(acac)_3 \cdot xH_2O$ (0.50 mmol), S_8 (0.032 mmol), Na(oleate) (0.50 mmol), OM (17 mmol), OA (2.5 mmol) and ODE (32.5 mmol) were placed in a 100 mL three-neck flask at room temperature. The yellow solution was heated to 120 °C under vacuum for 20 min to remove water and other impurities with low boiling points. The mixture was then heated to 310 °C and stirred at this temperature for 30 min under purified N_2. The transparent solution gradually became turbid starting from 280 °C. Then the mixture was left to cool to room temperature under N_2. The nanoparticles were isolated by centrifugation using ethanol and washed at least three times using a THF/ethanol (1/5) mixture to remove the remaining reagents and organic matter.

Thermogravimetric analysis coupled with mass spectrometry (TGA-MS)

Thermogravimetry analysis (TGA) (Netzsch STA449F3 Jupiter apparatus) coupled with a quadrupole mass spectrometry (MS) (Aëolos QMS403D, 70 eV, electron ionisation) *via* a heated capillary system was used to monitor the decomposition of samples during the annealing process and to analyze the evolved gaseous species. Before each experiment, the TGA system was first evacuated and then flushed with the same ultrahigh purity gas which was used for the thermal treatment. The experiments were carried out under dynamic inert or

reactive gas: He (99.999 % purity) or 20 % O_2 in He (99.999 % purity) at a flow rate of 50 cm^3/min. The samples were heated in Al_2O_3 crucibles up to 900 °C or 1200 °C with a heating rate at 2 °C/min.

X-ray Powder Diffraction (XRD)

The different X-ray diffraction patterns of dry powders were measured on a Bruker D8 diffractometer using Cu Kα radiation at 1.5406 Å. Typical diffractograms were collected with steps of 0.05 ° and a scanning speed of 5 s/point. The backgrounds of the patterns were subtracted using the EVA software.

Fourier Transform Infrared Spectroscopy (FTIR)

Infrared spectra were collected on a Spectrum 400 (PERKINELMER) spectrometer. The dry sample (1 to 3 mg) was deposited on the attenuated total reflectance (ATR) crystal. Transmittance was measured between 4000 cm^{-1} and 550 cm^{-1} with steps of 0.5 cm^{-1}.

Acknowledgements

This work was supported by French state funds managed by the ANR within the Investissements d'Avenir programme under reference ANR-11-IDEX-0004-02, and more specifically within the framework of the Cluster of Excellence MATISSE led by Sorbonne Université. Sorbonne Université, CNRS, and the Collège de France are acknowledged for financial support. We acknowledge the National Center for Electron Microscopy (UCM) for assistance with the generation of electron microscopy data.

Table of Content

Capping ligands play an important role in the chemistry of nanoparticles and their biomedical applications. We show that the thermal stability of oleate-covered $Gd_2O_2S_x$ nanocrystals is limited and strongly depends on the annealing atmosphere (inert or oxidizing). Annealing the nanoparticles in air enables removing the ligands without altering the nanocrystals structure. This work establishes the range of conditions for their practical use and provides an access to ligand-free nanoparticles.

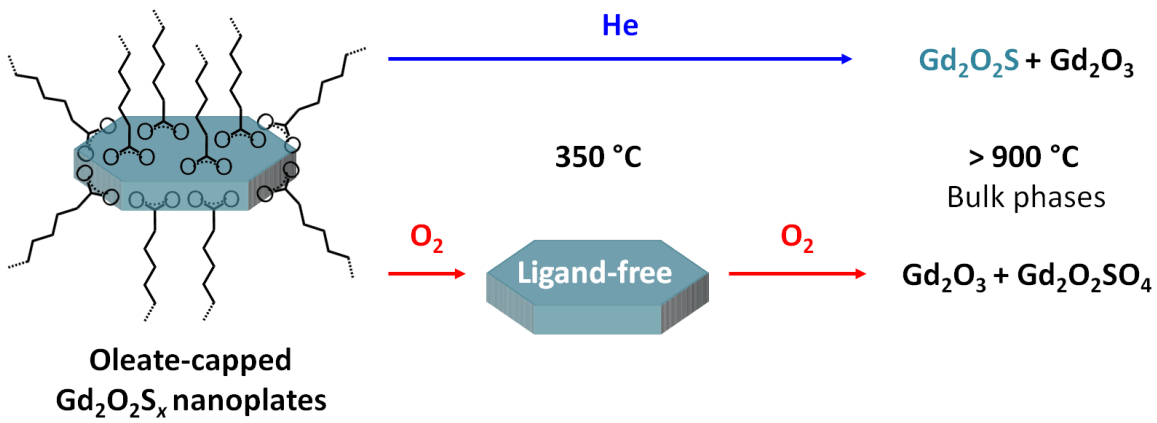

References

(1) Royce, M. R. U.S. Patent N°3418246, 1968.

(2) Jüstel, T.; Nikol, H.; Ronda, C. *Angew. Chemie Int. Ed.* **1998**, *37* (22), 3084–3103.

(3) Ronda, C. .; Jüstel, T.; Nikol, H. *J. Alloys Compd.* **1998**, *275–277*, 669–676.

(4) Strel'tsov, A. V.; Dmitrienko, V. P.; Dmitrienko, A. O.; Gulyaev, Y. V.; Sinitsyn, N. I.; Torgashov, G. V. *J. Commun. Technol. Electron.* **2009**, *54* (4), 487–492.

(5) Brixner, L. H. *Mater. Chem. Phys.* **1987**, *16* (3–4), 253–281.

(6) Rossner, W.; Grabmaier, B. C. *J. Lumin.* **1991**, *48–49* (1), 29–36.

(7) Michail, C. M.; Fountos, G. P.; Liaparinos, P. F.; Kalyvas, N. E.; Valais, I.; Kandarakis, I. S.; Panayiotakis, G. S. *Med. Phys.* **2010**, *37*, 3694–3703.

(8) Alves, R. V.; Buchanan, R. A.; Wickersheim, K. A.; Yates, E. A. C. *J. Appl. Phys.* **1971**, *42* (8), 3043–3048.

(9) Markushev, V. M.; Ter-Gabriélyan, N. É.; Briskina, C. M.; Belan, V. R.; Zolin, V. F. *Sov. J. Quantum Electron.* **1990**, *20* (7), 773–777.

(10) Iparraguirre, I.; Azkargorta, J.; Merdrignac-Conanec, O.; Al-Saleh, M.; Chlique, C.; Zhang, X.; Balda, R.; Fernández, J. *Opt. Express* **2012**, *20* (21), 23690.

(11) Zhu, K.; Ding, W.; Sun, W.; Han, P.; Wang, L.; Zhang, Q. *J. Mater. Sci. Mater. Electron.* **2016**, *27* (3), 2379–2384.

(12) Sun, W.; Zhu, K.; Xu, H.; Yang, X.; Yu, M.; Li, X.; Wang, L.; Zhang, Q. *J. Mater. Sci. Mater. Electron.* **2017**, *28* (1), 697–701.

(13) Larquet, C.; Klein, Y.; Hrabovsky, D.; Gauzzi, A.; Sanchez, C.; Carenco, S. *Eur. J. Inorg. Chem.* **2019**.

(14) Hernández-Adame, L.; Méndez-Blas, A.; Ruiz-García, J.; Vega-Acosta, J. R.; Medellín-Rodríguez, F. J.; Palestino, G. *Chem. Eng. J.* **2014**, *258* (6), 136–145.

(15) Tian, Y.; Lu, F.; Xing, M.; Ran, J.; Fu, Y.; Peng, Y.; Luo, X. *Opt. Mater. (Amst).* **2017**,

64, 58–63.

(16) Bagheri, A.; Rezaee Ebrahim Saraee, K.; Shakur, H. R.; Zamani Zeinali, H. *Appl. Phys. A Mater. Sci. Process.* **2016**, *122* (5), 1–8.

(17) Thirumalai, J.; Chandramohan, R.; Divakar, R.; Mohandas, E.; Sekar, M.; Parameswaran, P. *Nanotechnology* **2008**, *19* (39), 395703.

(18) Li, W.; Liu, Y.; Ai, P.; Chen, X. *J. Rare Earths* **2009**, *27* (6), 895–899.

(19) Osseni, S. A.; Lechevallier, S.; Verelst, M.; Dujardin, C.; Dexpert-Ghys, J.; Neumeyer, D.; Leclercq, M.; Baaziz, H.; Cussac, D.; Santran, V.; Mauricot, R. *J. Mater. Chem.* **2011**, *21* (45), 18365.

(20) Thomson, J. W.; Nagashima, K.; Macdonald, P. M.; Ozin, G. a. *J. Am. Chem. Soc.* **2011**, *133* (13), 5036–5041.

(21) Ding, Y.; Gu, J.; Ke, J.; Zhang, Y.-W.; Yan, C.-H. *Angew. Chemie Int. Ed.* **2011**, *50* (51), 12330–12334.

(22) Larquet, C.; Nguyen, A.-M.; Ávila-Gutiérrez, M.; Tinat, L.; Lassalle-Kaiser, B.; Gallet, J.-J.; Bournel, F.; Gauzzi, A.; Sanchez, C.; Carenco, S. *Inorg. Chem.* **2017**, *56* (22), 14227–14236.

(23) Lei, L.; Zhang, S.; Xia, H.; Tian, Y.; Zhang, J.; Xu, S. *Nanoscale* **2017**, *9* (17), 5718–5724.

(24) Zhang, T.; Gu, J.; Ding, Y.; Zhang, Y.-W.; Yan, C.-H. *Chempluschem* **2013**, *78* (6), 515–521.

(25) Xing, M.; Cao, W.; Pang, T.; Ling, X. *Solid State Commun.* **2009**, *149* (23–24), 911–914.

(26) Song, Y.; You, H.; Huang, Y.; Yang, M.; Zheng, Y.; Zhang, L.; Guo, N. *Inorg. Chem.* **2010**, *49* (24), 11499–11504.

(27) Wang, G.; Zou, H.; Zhang, B.; Sun, Y.; Huo, Q.; Xu, X.; Zhou, B. *Opt. Mater. (Amst).*

2015, *45*, 131–135.

(28) Flahaut, J.; Guittard, M.; Patrie, M. *Bull. Soc. Chim. Fr.* **1958**, *7*, 990–994.

(29) He, W.; Osmulski, M. E.; Lin, J.; Koktysh, D. S.; McBride, J. R.; Park, J.-H.; Dickerson, J. H. *J. Mater. Chem.* **2012**, *22* (33), 16728.

(30) Zhao, F.; Yuan, M.; Zhang, W.; Gao, S. *J. Am. Chem. Soc.* **2006**, *128* (36), 11758–11759.

(31) Carenco, S.; Labouille, S.; Bouchonnet, S.; Boissière, C.; Le Goff, X.-F.; Sanchez, C.; Mézailles, N. *Chem. - A Eur. J.* **2012**, *18* (44), 14165–14173.

(32) Sopoušek, J.; Pinkas, J.; Brož, P.; Buršík, J.; Vykoukal, V.; Škoda, D.; Stýskalík, A.; Zobač, O.; Vřešťál, J.; Hrdlička, A.; Šimbera, J. *J. Nanomater.* **2014**, *2014*, 1–13.

(33) NIST. Oleic acid mass spectrum (CAS: 112-80-1) https://webbook.nist.gov/cgi/cbook.cgi?ID=C112801&Units=SI&Mask=200#Mass-Spec.

(34) Deacon, G. B.; Phillips, R. J. *Coord. Chem. Rev.* **1980**, *33* (3), 227–250.

(35) Vaďura, R.; Kvapil, J. *Mater. Res. Bull.* **1971**, *6* (9), 865–873.

(36) Ribot, F.; Toledano, P.; Sanchez, C. *Inorganica Chim. Acta* **1991**, *185* (2), 239–245.

(37) Tong, L.; Lu, E.; Pichaandi, J.; Cao, P.; Nitz, M.; Winnik, M. A. *Chem. Mater.* **2015**, *27* (13), 4899–4910.

(38) Hauser, H.; Darke, A.; Phillips, M. C. *Eur. J. Biochem.* **1976**, *62* (2), 335–344.

(39) Anderson, N. C.; Hendricks, M. P.; Choi, J. J.; Owen, J. S. *J. Am. Chem. Soc.* **2013**, *135* (49), 18536–18548.

(40) Lüth, H.; Nyburg, S. C.; Robinson, P. M.; Scott, H. G. *Mol. Cryst. Liq. Cryst.* **1974**, *27* (3–4), 337–357.

(41) Ikeue, K.; Kawano, T.; Eto, M.; Zhang, D.; Machida, M. *J. Alloys Compd.* **2008**, *451* (1–2), 338–340.